Sample pH Can Drift During Native Mass Spectrometry Experiments: **Results from Ratiometric Fluorescence Imaging** Meagan M. Gadzuk-Shea, 1,2 Evan E. Hubbard, 1,3 Theresa A. Gozzo, 1 and Matthew F Bush 1* ¹ University of Washington, Department of Chemistry, Box 351700, Seattle, WA 98195-1700 ² orcid.org/0000-0001-9496-529X, Current Affiliation: Discovery Biology, Discovery Sciences, Biopharmaceuticals R&D, AstraZeneca, Waltham, MA 02451 ³ Current Affiliation: Current Affiliation: Department of Chemistry, University of California, Riverside, California 92521 *Address correspondence to mattbush@uw.edu

Abstract

The ability of nanoelectrospray ionization (nanoESI) to generate a continuous flow of charged droplets relies on the electrolytic nature of the process. This electrochemistry can lead to the accumulation of redox products in the sample solution. This consequence can have significant implications for native mass spectrometry (MS), which aims to probe the structures and interactions of biomolecules in solution. Here, ratiometric fluorescence imaging and a pH-sensitive, fluorescent probe are used to quantify changes in solution pH during nanoESI under conditions relevant to native MS. Results show that the extent and rate of change in sample pH depends on several experimental parameters. There is a strong correlation between the extent and rate of change in solution pH and the magnitude of both the nanoESI current and electrolyte concentration. Smaller changes in solution pH are observed during experiments when a negative potential is applied than for those when a positive potential is applied. Finally, we make specific recommendations for designing native MS experiments that control for these effects.

Introduction

36

37

38

39

40

41

42

43

44

45

46

47

48

49

50

51

52

53

54

55

56

57

58

The advent of electrospray ionization (ESI) made possible the analysis of large biomolecules by mass spectrometry (MS). In ESI, an analyte solution is in electrical contact with a potential that drives the generation of charged droplets. Conventional ESI uses metal capillaries with large (hundreds of µm) orifices that require external pumping to flow solutions and applied potentials of several kV to generate charged droplets. These conditions can result in poor ionization efficiency and analyte aggregation due to the formation of large droplets.² nanoESI addressed these specific challenges by generating much smaller droplets (≤ 200 nm in diameter)³ than those produced by conventional ESI (typically >1 µm in diameter).⁴ Generally, nanoESI utilizes borosilicate glass or fused silica capillaries that have been pulled to a tip of 1 to 10 µm. Applying a potential of less than 1.5 kV is usually sufficient to generate a Taylor cone, and the transport of the sample solution can be maintained through electrokinetic flow, without applying additional pressure.⁵ Flow rates in nanoESI devices are typically tens of nL·min⁻¹ and depend on the composition of the solvent, the tip orifice diameter, the distance to counter electrode (typically the inlet to the mass spectrometer), and the electrospray potential.^{2,6–8} For comparison, flow rates in conventional ESI sources are typically >1 μL·min⁻¹ and are controlled by external pumping.^{6,8} Native MS is used to study the structures and interactions of biomolecules^{9,10} and usually makes use of nanoESI.¹¹ In native MS, protein ions are generated from solutions with ionic strength and pH similar to those of the relevant biological environment. Ionic strength affects electrostatic interactions within and between molecules, e.g., the p K_a values of amino acids in proteins depend on ionic strength¹² and increasing the concentration of NaCl from 20 to 600 mM is associated with both a tenfold increase in the rate of amyloid formation for islet amyloid

polypeptide¹³ and a thirtyfold decrease in the activity of the Na,K-ATPase.¹⁴ Ammonium acetate is widely used as an electrolyte due to its volatility, which makes it particularly amenable to MS. Buffers are most effective at pH values near the relevant pK_a .¹⁵ Although the combination of aqueous ammonia (pK_a 9.25) and acetic acid (pK_a 4.8) results in a mixture that is close to neutral pH, ¹⁶ that solution will be ineffective at resisting changes in pH. In contrast, ammonium phosphate has a $pK_{a,2}$ of 7.4 and buffers well at neutral pH, but obtaining well-resolved native mass spectra from solutions of aqueous ammonium phosphate has only been demonstrated using submicron emitters.¹⁷ Submicron emitters have enabled exciting new measurements of noncovalent interactions in solution with reduced extents of nonspecific aggregation during ESI;^{18,19} however, surface-induced unfolding of proteins²⁰ and emitter clogging have also been reported for those experiments. Aqueous ammonium bicarbonate is another popular option for native MS, but the unfolding of proteins^{21,22} has also been reported for some experiments using this salt.

During ESI, application of a potential to the solution causes electrophoretic separation of the charged solutes. Ions with the same polarity as the applied potential move toward the exit of the capillary, and charged droplets are released in a Taylor cone when the Coulombic repulsion at the tip exceeds the surface tension of the liquid.³ Through solvent evaporation and fission events, these charged droplets become bare ions that can be detected by a mass spectrometer.²³ Generating this continuous flow of unipolar, charged droplets requires that charge-balancing reactions occur in the sample solution.^{24,25} For example, when a positive potential is applied, net positive charge is expelled, and only electrons flow through the electrode, it follows that electrons must be produced within the solution.^{25,26} Charge balancing occurs through redox reactions.^{27–30} The specific redox reactions that occur during electrospray are determined by a

complex interaction of experimental parameters such as flow rate, concentration of electrolytes, magnitude of electrospray current, and redox properties of the species present.^{28,29} Even when only considering water and the applicable acid/base and redox products, Van Berkel and coworkers proposed a dozen redox reactions that are likely relevant to electrospray.³¹ The electrochemistry of samples for native MS, which include many additional molecules and ions, would be even more challenging to understand.

Although electrochemistry undoubtedly occurs during ESI, the implications and significance of electrochemistry on measurements remains uncertain. ^{29,32} Application of positive potentials to zinc or iron electrodes results in the appearance of Zn²⁺ or Fe²⁺ in the respective mass spectra. ³³ Absorbance of a porphyrin solution measured as a function of electrospray parameters revealed the extent of oxidation that had occurred in those experiments. ³⁴ Changes in solution composition can also affect redox chemistry occurring during electrospray. ^{27,30,35} The electrochemistry concomitant with electrospray has been leveraged for the analysis of molecules otherwise challenging to ionize, such as metallocenes, fullerenes, and inorganic compounds. ^{36–40} Changes in the pH of droplets generated by ESI have been probed using ratiometric fluorescence ⁴¹ and MS⁴² based methods; these studies established that the pH of electrospray-produced droplets can be very different than the original samples.

Despite the obvious occurrence of redox-induced changes in pH, little work has examined pH change in solution conditions utilized for native MS. Native MS experiments usually strive to probe the structures and interactions of biological molecules in solution, but any changes in sample pH during experiments may affect the properties of interest. For example, the dissociation constant of the dimer of the α -crystallin domain of HSPB5 increases by a factor of 15 between pH 7.5 and 6.5.⁴³ Native MS is also increasingly used to study the aggregation of

many intrinsically disordered proteins,⁴⁴ such as the Alzheimer's disease related α-synuclein, but aggregation can depend strongly on pH.⁴⁵ Therefore, it is of great interest to determine to what extent these changes occur and to devise schemes to mitigate these changes. In this work, we will quantify the changes in pH of solutions typically implemented in native-MS experiments using nanoESI in both positive and negative ionization modes. It is widely believed that the structures of native-like ions depend on the structures of the biological molecules in solution prior to ionization.⁴⁶⁻⁴⁸ Therefore, we specifically probe the pH of the bulk solution inside the nanoESI capillary. We characterize changes in sample pH as a function of time, ionization currents, electrolyte concentrations, and polarities, using ranges of parameters that encompass most native MS experiments.

Methods

Native Mass Spectrometry. Concanavalin A was purchased as a lyophilized powder from Sigma-Aldrich (Item #C2010, St. Louis, MO). The material was dissolved at to a concentration of 40 μM monomer in aqueous 200 mM ammonium acetate at pH 7.0, divided into 20 μL aliquots, and flash frozen. Prior to use, one aliquot was thawed and exchanged into aqueous 10 mM ammonium acetate at pH 6.0 or pH 7.0 using Micro Bio-Spin 6 columns (Bio-Rad, Hercules, CA), then diluted to final concentrations of 16 μM monomer with the same solvent. Approximately 2 μL of solution was loaded into a borosilicate capillary (1.00 mm outer diameter, 0.78 mm inner diameter) that was pulled to a 1 to 3 μm tip (Sutter Instruments P-97). A platinum wire was inserted through the wide end of the capillary to make electrical contact with the solution. Electrospray was achieved by applying 0.65 to 1.2 kV of potential to the wire to establish and maintain an ionization current of 60 nA. The current was measured using the

voltage drop across a multimeter that was positioned in series with the potential that was applied to the wire. Mass spectra were acquired using a Cyclic Ion Mobility-Mass Spectrometry System (Waters Co., Wilmslow, U.K.).⁴⁹

Samples for Ratiometric Fluorescence Imaging. SNARF-4F 5-(and-6)-carboxylic acid, which will be referred to as SNARF-4F, 50,51 was purchased from Fisher Scientific (Rockwood, TN) as a lyophilized solid. A stock solution was prepared by dissolving the solid in 18.6 M Ω water to a concentration of 2 mM. Aliquots containing 5 μ L of stock solution were kept frozen at $-80~^{\circ}$ C or $-18~^{\circ}$ C and protected from light until use. Prior to experiments, one aliquot was thawed and diluted to a final concentration of 1 μ M. Solutions were prepared as follows: aqueous ammonium acetate solutions were prepared at 200 mM and 1 M concentration; 10 mM solutions were prepared through serial dilution of the 200 mM solution. The pHs of solutions were adjusted with solutions of hydrochloric acid or ammonium hydroxide of the same concentration as the electrolyte in the solution being adjusted. Figure 1 shows the fluorescence spectra upon excitation at 530 nm of SNARF-4F in aqueous 200 mM ammonium acetate acquired as a function of pH.

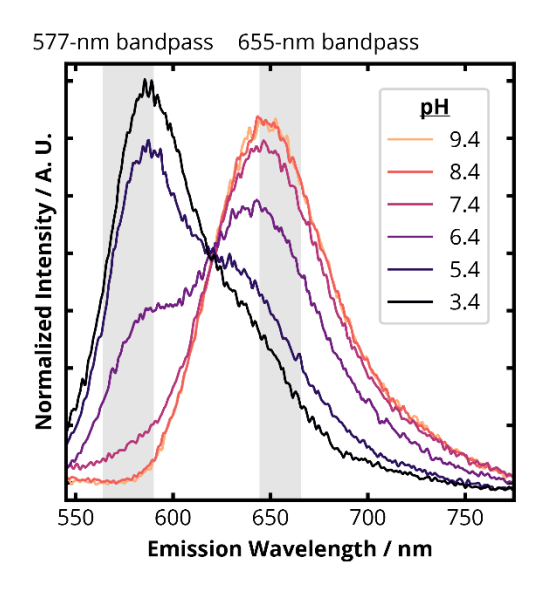
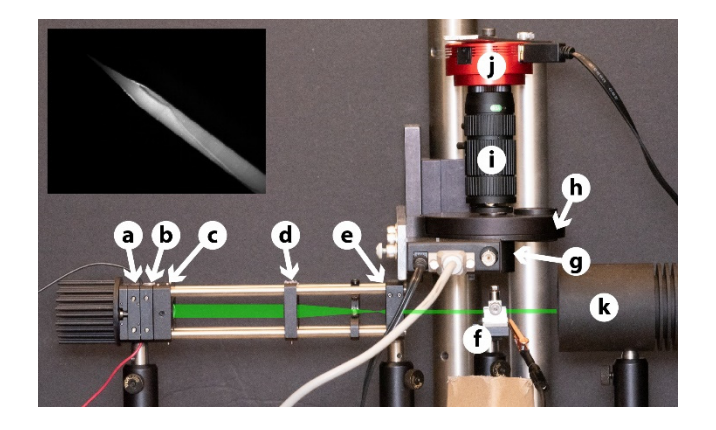


Figure 1. Fluorescence spectra of SNARF-4F prepared in solutions of aqueous 200 mM ammonium acetate solutions that were adjusted to the indicated pH values. Emission spectra were collected with a luminescence spectrophotometer (Perkin Elmer LS-50B, Walham, MA) using an excitation wavelength of 530 nm. At the lowest pH, 3.4, excitation of SNARF-4F results in an emission spectrum with maximum relative intensity around 585 nm and a less intense shoulder at longer wavelengths. The feature at 585 nm decreases in intensity with increasing solution pH (almost disappearing by pH 7.4), and the longer-wavelength feature increases in relative intensity and appears centered near 652 nm. These spectra were used to select bandpass filters centered near 577 and 655 nm; the shaded regions span the approximate transmission windows of those filters. Additional aspects of photophysics of SNARF-4F, as well as the structures of the acid and conjugate base forms, have been reported previously.⁵¹

Experimental Setup. To probe the pH of samples during electrospray, we developed the apparatus that is shown in Figure 2 and described below. Fluorescence was initiated by illuminating the sample with 530-nm light generated by a light-emitting diode operated with a current of 1 A, which yields ~60 mW of light (Figure S1). Software was written to synchronize the light source, the filter wheel, and the camera. For each time point, two images were collected using each bandpass filter. Images were collected with an exposure time of 400 ms and a gain of zero. For most experiments, fluorescence images were recorded every 25 seconds for 125 iterations. During rotation of the filter wheel, the light source was switched off to minimize photobleaching of SNARF-4F.



165

166

167

168

169

170

171

172

173

174

175

176

177

178

179

180

Figure 2. Photograph of apparatus used for these experiments. Light was generated by a 530-nm, light-emitting diode (a), passed through a 525-nm bandpass filter (b), and collimated using an aspheric condenser lens with a focal length of 20 mm (c). That light was then focused using a plano-convex lens with a focal length of 75 mm (d), recollimated using a second aspheric condenser lens with a focal length of 20 mm (e), and then used to irradiate the sample capillary (f). A fraction of the emitted light was passed through a long-pass filter (g) into a filter wheel (h) containing bandpass filters centered near 577 nm and 655 nm, which were selected based on the pH-dependent, fluorescence spectra of SNARF-4F (Figure 1). The transmitted light was focused using a lens (i) and detected using a monochromatic CMOS camera (j). To minimize stray light in these experiments, the camera was mounted at an angle of $\sim 12^{\circ}$ relative to the sample capillary, a beam dump (k) was positioned in line with the incident light, and the apparatus was operated in an enclosed box constructed of foam board with a matte, black coating. The green region is a crude approximation of the beam path of the 530-nm light in these experiments. Inset is a representative image of a capillary containing 500 nM SNARF-4F that was acquired using the 655-nm bandpass filter. Additional details, including part numbers and manufacturers, are included in the Supporting Information.

182

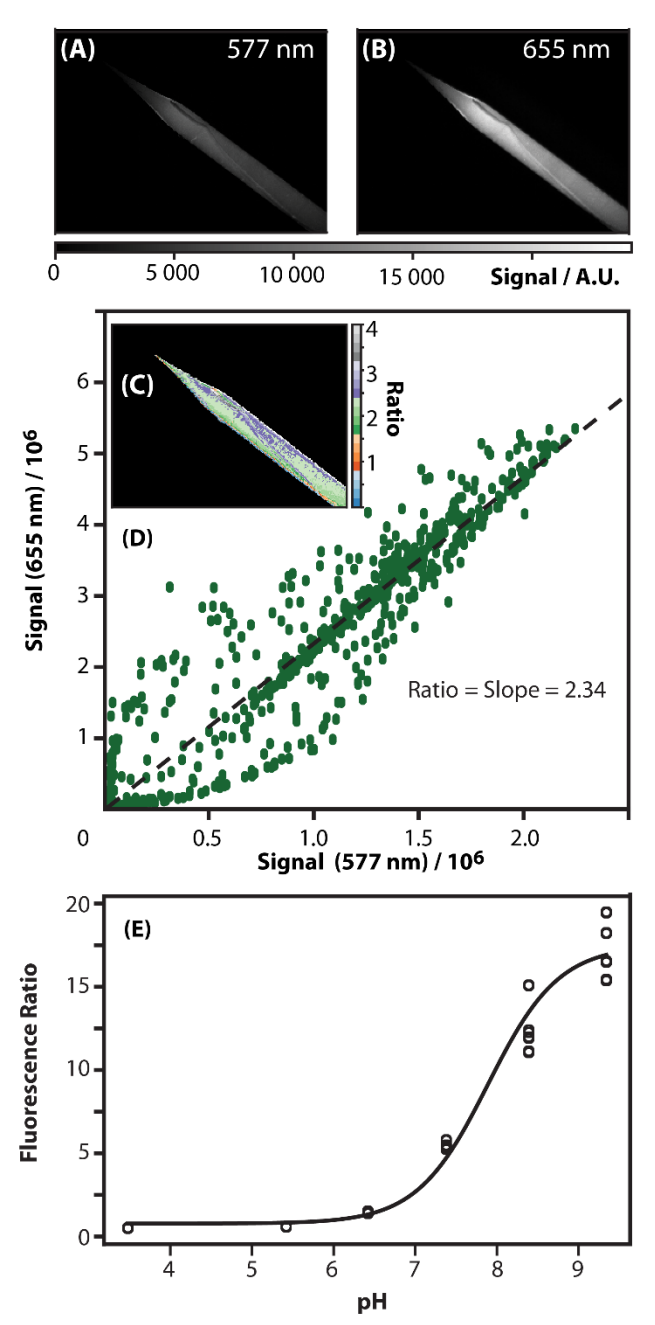
Data Acquisition and Processing. Ratiometric analysis of the fluorescence intensity of SNARF-4F at 577 nm (Figure 3A) and 655 nm (Figure 3B) was performed to relate the measurements to solution pH. The intensities of two images acquired in succession were added, and then, the resulting data was binned with a block size of 4 or 16 pixels and masked using minimum (to exclude pixels that did not probe the capillary) and maximum (to exclude a few "hot" pixels on the sensor) thresholds (Figure 3C). The intensity of fluorescence at 655 nm was plotted against the fluorescence intensity at 577 nm (Figure 3D). The slope resulting from regression analysis of these data was taken as the experimental ratio.

Calibration. Figure 3E shows the ratio of fluorescence at 655 nm relative to 577 nm (R), which was recorded six times for each standard. Measurements were performed in a pseudorandom order to minimize systemic biases. Each measurement used a new borosilicate capillary, and the platinum wire was rinsed with 18.6 M Ω water prior to insertion into the solution-containing capillary, although no potential was applied. These steps were taken to capture the variability in the experimental measurements. The expected relationship between pH and R is given by Equation 1:⁵²

$$pH = K + log\left(\frac{R - R_A}{R_B - R}\right)$$
 (Equation 1)

where R_A is the ratio for the acid form of SNARF-4F, R_B is the ratio for the conjugate base form of SNARF-4F, and K is a constant that depends on the p K_A of SNARF-4F, the signal for the acid form of SNARF-4F at 577 nm, and the signal for the conjugate base form of SNARF-4F at 655 nm. For calibration, experimental values of R were plotted as a function of pH. The Levenberg-Marquardt method was then used to determine the values of K, R_A , and R_B that minimize the least-squares difference between the experimental values of R and those expected based on the model in Equation 1. The values of K, R_A , and R_B determined for the calibration curve shown in

Figure 3E were used to determine the "apparent pH" for all other ratiometric fluorescence measurements.



206

207

226

227

228

Figure 3. Panels A-D show representative data for a single measurement of the fluorescence ratio. (A) Fluorescent image acquired using the 577-nm bandpass filter. (B) Fluorescent image acquired using the 655-nm bandpass filter. The intensity for neighboring pixels were binned and then masked using thresholds. (C) The ratio of the intensity using the 655-nm bandpass filter to that using the 577-nm bandpass filter for each binned pixel. (D) The intensity using the 655-nm bandpass filter was plotted as function of the intensity using the 577-nm bandpass filter for each binned pixels; the slope for that data was used to determine fluorescence ratio for that pair of images. (E) Calibration curve generated from measuring the fluorescence ratio of SNARF-4F

standards and Equation 1. Standard solutions of 500 nM SNARF-4F were prepared in aqueous 200 mM ammonium phosphate at pH values of 3.5, 5.4, 6.4, 7.4, 8.4, and 9.3, as measured using a calibrated pH probe. Aqueous ammonium phosphate, rather than ammonium acetate, standards

were used for these experiments based on the increased buffering capacity of the former near neutral pH.

Electrospray Experiments. Approximately 10 μL of solution was loaded into a borosilicate capillary (1.00 mm outer diameter, 0.78 mm inner diameter) that was pulled to a 1 to 3 μm tip (Sutter Instruments P-97). A platinum wire was inserted through the wide end of the capillary to make electrical contact with the solution. Electrospray was achieved by applying 0.7 to 2.7 kV of potential to the wire using a power supply (Bertan 205B-03R, Hicksville, NY). Ions were collected on a stainless-steel plate positioned ~10 mm from the capillary tip and the current of the collected ions was measured using a picoammeter (Keithley 485, Cleveland, OH). The magnitude of applied potential was adjusted to maintain a relatively constant electrospray current (±10 nA). Any experiments that exhibited erratic current were terminated and a new tip loaded.

Results and Discussion

Native Mass Spectra Can Depend on Acquisition Time. Concanavalin A is a carbohydrate-binding protein that forms predominantly dimers and tetramers in solution near neutral pH; the relative abundance of tetramer increases with pH. 53,54 Figure 4A shows the initial native mass spectrum acquired for a sample of concanavalin A that was prepared in aqueous 10 mM ammonium acetate at pH 7.0 using an electrospray current of 60 nA. The predominant peaks in the spectrum are assigned to dimers and tetramers of concanavalin A. The sum of the intensities of the tetramer ions is roughly threefold greater than that for the dimer ions (\sum tetramer / \sum dimer = 2.97). Figure 4B shows the mass spectrum that was acquired during the same experiment but after 30 minutes of ionization. The sum of the intensities of the tetramer

ions is roughly equal to that of the dimer ions (\sum tetramer / \sum dimer = 1.01). For comparison, Figure 4C shows the initial native mass spectrum for a similar sample but prepared at pH 6.0. The relative intensities of the dimer and tetramer (\sum tetramer / \sum dimer = 0.82) are more similar to those in Figure 4B. Several replicate measurements of the sample prepared at pH 7 were acquired and all exhibit decreasing tetramer fraction with increasing time (Figure 4D). Although many native MS experiments only generate ions from individual samples for a short length of time, others do so for much longer durations, *e.g.*, experiments that acquire data as a function of collision energy^{55,56} or temperature⁵⁷ or that generate product ions through many different channels.^{48,58} Based on these (Figure 4) and other (not shown) results, we hypothesized that the electrospray solutions were becoming acidified with increasing acquisition time.

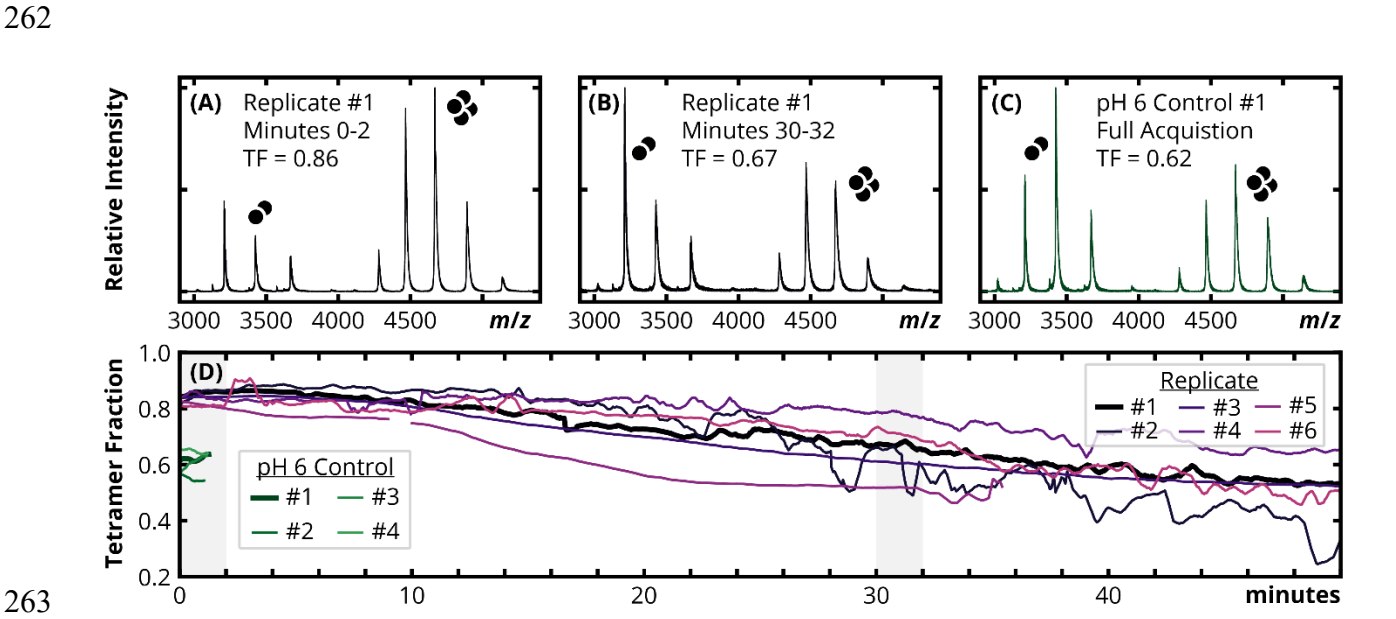


Figure 4. Native mass spectrometry of concanavalin A samples prepared in aqueous 10 mM ammonium acetate. Representative mass spectra of a sample prepared at pH 7.0 that were acquired (A) initially and (B) after 30 minutes (B) of ionization. The peaks in this *m/z* range were assigned as indicated to dimers and tetramers; there were also lower-intensity, lower-*m/z* peaks that were assigned to the monomer. (C) Representative mass spectrum of a sample prepared at

pH 6.0. Tetramer fraction, TF, is defined as sum of intensities of the tetramer ions (those with m/z between 4250 and 5400) divided by the sum of the intensities of the dimer (those with m/z between 3000 and 3900) and tetramer ions; all intensities were weighted by oligomeric state. (D) Tetramer fraction as a function of ionization time for 6 technical replicates of the sample prepared at pH 7.0; the tetramer faction decreases with increasing ionization time for all replicates. Results for 4 samples prepared at pH 6.0 are shown for comparison. All experiments used an electrospray current of 60 nA.

The objective of this study was to develop a quantitative understanding of the effects of electrospray on the pH of samples during native MS experiments. This objective is significant because it is well understood that electrochemistry occurs during electrospray ionization and that the structures, interactions, and activity of biological molecules can depend strongly on pH. Towards this objective, we used a pH-dependent, fluorescent probe and ratiometric fluorescence imaging of samples during ion generation. Ratiometric analysis of the fluorescence signals were then used to relate measurements and solution pH. Specifically, we characterized sample pH as a function of electrospray current, electrolyte concentration, and electrospray polarity.

Measuring the pH of Solutions Inside nanoESI Capillaries. Measuring the pH of solutions inside nanoESI capillaries during ionization presents several challenges. For example, the small capillary dimensions and large applied potentials would hinder potentiometric measurements. The capillary shape and the need for capillary repositioning would pose obstacles to calibrating a single optical signal from a probe molecule. Factors such as illumination intensity, sample thickness, and probe concentration can influence a single optical signal, and probe concentration may change over time due to photobleaching. To address these challenges,

we used ratiometric fluorescence imaging, as described in the *Methods* section. This technique involves imaging emission at two different wavelengths and using the ratio of those signals to estimate the sample pH. Since many of the factors that impact emission intensity are common to measurements at both wavelengths, the use of ratios helps minimize their influence on the measurement. For the probe molecule, we selected SNARF-4F, which exhibits pH-dependent emission spectra (Figure 1) that make it "exceptionally suitable for pH measurement in the range from about 6.0 to 7.5" and appealing for use in quantitative imaging. SNARF-1, a related molecule with analogous photophysical properties but a larger p K_a , has been used to probe pH changes that occur during the evaporation of ESI droplet.

Briefly, nanoESI capillaries loaded with solutions containing SNARF-4F were irradiated with 530-nm light; the resulting emission was filtered with bandpass filters centered at either 577 or 655 nm and imaged on a CMOS sensor (Figure 2). These bandpass filters were selected based on the emission spectra of SNARF-4F in a series of aqueous ammonium acetate standards with a range of pH values (Figure 1). The ratiometric response of SNARF-4F as a function of solution pH was determined from the analysis of standards (Figure 3A-3D) prepared at selected values of pH. Plotting the ratio as a function of pH yielded a sigmoidal relationship, with the steepest region falling between pH values of ~ 6.5 and 8.5 (Figure 3E). The observed response is consistent with the expected acid-base equilibria⁶⁰ and previous pH-dependent measurements of SNARF-4F using other fluorescence measurements. This response curve was used to parameterize Equation 1. Replicate measurements were used to characterize inter-experiment variability, as described in the *Methods* and *Supporting Information*. This analysis suggests that this method is most appropriate for ratios that correspond to pH values between 6 and 8. Because the relationship between the ratio and the apparent pH is less-well defined outside of this range

of pH values, subsequent results will be plotted linearly along the vertical axis using the measurand (the fluorescence ratio), and the corresponding apparent pH values will be indicated to the right of figures. We did not attempt to estimate pH for very-low values of ratio, given the sigmoidal behavior of the calibration curve (Figure 3E).

ammonium acetate at neutral pH and use positive ionization mode with a modest electrospray current. $^{2.9,61}$ Because of the prevalence of these conditions, "status quo" will be used to describe experiments performed using an aqueous 200 mM ammonium acetate at pH 7.0, positive polarity, and 60 nA current. Additionally, a surplus of replicates under these "status quo" conditions were performed spanning multiple weeks and sample preparations to capture the inherent measurement variability. To aid in discussion of the results, the experiment is presented in four regions with the first three regions corresponding to 10-minute intervals, and a fourth region from 30 minutes onwards. Note that all emitters in this study were initially loaded with approximately $10 \mu L$ of solution. Many native MS studies use smaller sample volumes, e.g., $1-2^{61}$ or $1-5^{62}$ μL . Therefore, the rates of change in the present study are likely to be slower than would be expected during many native MS experiments.

Figure 5 shows the results from many "status quo" replicates. Under these conditions, the solutions displayed an initial fluorescence ratio of 2.41 (95% CI: 2.35-2.47) corresponding to an apparent pH of 6.92 (95% CI: 6.91-6.94). During the first 10 minutes of electrospray (region I) the solutions exhibit a slow decrease in fluorescence ratio averaging $-0.02 \, \text{min}^{-1}$. In region II, 10-20 minutes, the rate of change in fluorescence ratio increases to $-0.06 \, \text{min}^{-1}$. Region III is similar, exhibiting an average change of $-0.05 \, \text{min}^{-1}$. Region IV reveals significant slowing to $-0.02 \, \text{min}^{-1}$ and apparent leveling of the ratio is observed at the conclusion of the experiment.

All status-quo experiments result in a decrease in apparent pH of over 1 pH unit; on average, the apparent pH decreases below 6 after 34 minutes. For context, a 1 pH unit decrease in pH causes the dissociation constant of the dimer of the α -crystallin domain of HSPB5 to increase by a factor of 15.⁴³ We attribute the increased stability of fluorescence ratios at longer times (and lower pH) to (1) increased buffering at lower pH by acetic acid, which has a p K_a of 4.8, and (2) the sigmoidal relationship between fluorescence ratio and pH.

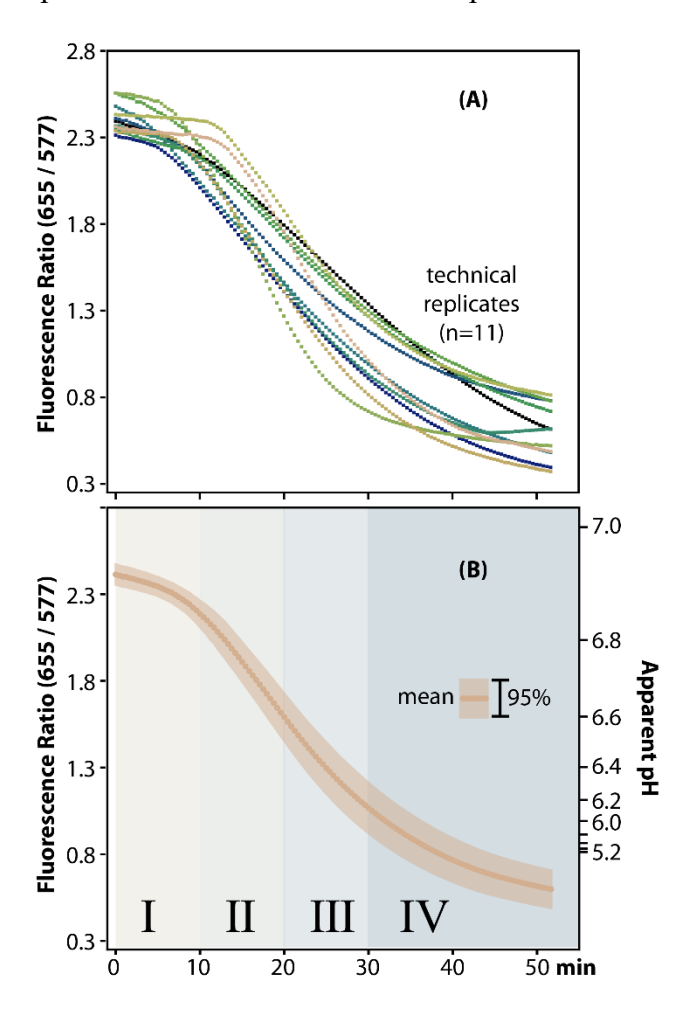


Figure 5. Ratiometric analysis of the fluorescence intensity for a solution of aqueous 200 mM ammonium acetate measured as a function of time using an electrospray current of 60 nA. All solutions initially had a pH of 7.0. (A) Over a 52-minute period, 125 sets of images capturing the fluorescence of SNARF-4F at 655 nm and 577 nm are recorded. (B) The corresponding apparent

pH determined as described in the *Methods* using the data in Figure 3E. The mean and 95% CI of 11 technical replicates are shown. The shaded blocks represent time regions I-IV, which are used to organize observations in the discussion.

Note that there is significant variance among the technical replicates shown in Figure 5. We attribute a significant fraction of this variance to small differences in the position of the sample capillary, which has a shape that causes significant scattering of the excitation light and presents different thicknesses of capillary and sample for imaging. As discussed in the *Methods* section, we used several approaches to minimize variance, including the use of ratiometic fluorescence, quantifying the fluorescence ratio on a pixel-by-pixel basis, offsetting the angle between the capillary and the camera, and by positioning multiple optical filters between the capillary and the camera. There are likely additional factors, *e.g.*, fouling of the platinum wire electrode, that contribute to differences between technical replicates. Such factors may also contribute to the variance in the native MS results reported in Figure 4D. Although the variance should be considered while evaluating these results, the magnitude of the change in fluorescence ratio is much larger than that of the variance between technical replicates.

Effect of Electrospray Current. To characterize the effects of electrospray current on the pH of solutions during native MS experiments, we performed experiments that only varied the magnitude of that parameter. Although most native MS studies do not report electrospray currents, most studies do report electrospray voltage and values between 0.7 kV and 2.0 kV are common.^{2,61} The width of this range suggests that different studies fall under different current regimes. We used a low current of 30 nA, a moderate current of 60 nA, and a high current of 120 nA; these values are within the range of currents that have been reported.^{2,63} Figure 6 shows

fluorescence response over time at each current. There is a clear relationship between the onset and magnitude of change in fluorescence ratio and the magnitude of the electrospray current.

During region I, the smallest current (30 nA, blue traces) exhibits the slowest change in fluorescence ratio and the largest current (120 nA, green traces) displays the most dramatic change in fluorescence ratio. An intermediate amount of current (60 nA, beige interval) falls in between the two extremes. However, beyond region I, the rate of change in fluorescence ratio for all three currents is relatively similar. In region IV, the rate of change slows in all three cases, with 120 nA leveling off the most dramatically, although it exhibits the greatest overall change in fluorescence ratio relative to the other currents. The slower response at 30 nA current is consistent with slower production of redox products at lower currents. Note that one technical replicate at 30 nA exhibits a prolonged resistance to change in pH; that data was acquired using the same protocol and the origin of the apparent resistance in that replicate is not understood.

Overall, all currents result in a substantial decrease in fluorescence ratio (*i.e.*, acidification) during electrospray, although at different rates and to varying extents. The highest magnitude of current, 120 nA, displays an 85% decrease in fluorescence ratio and 60 nA and 30 nA decrease 74% and 65%, respectively. This corresponds to a decrease of more than 1 pH unit in all three cases. The 1 pH unit decrease occurs after just 20 minutes at 120 nA. These results demonstrate that using lower electrospray currents in nanoESI can delay the onset of acidification. Note that some analysts initially apply a much higher electrospray voltage to assist in establishing a stable spray prior to lowering the voltage prior to acquiring data. Whereas the results for lower current exhibit slow initial changes, the results for 120 nA suggest that using higher currents may rapidly reduce the capacity of the sample to resist changes in pH.

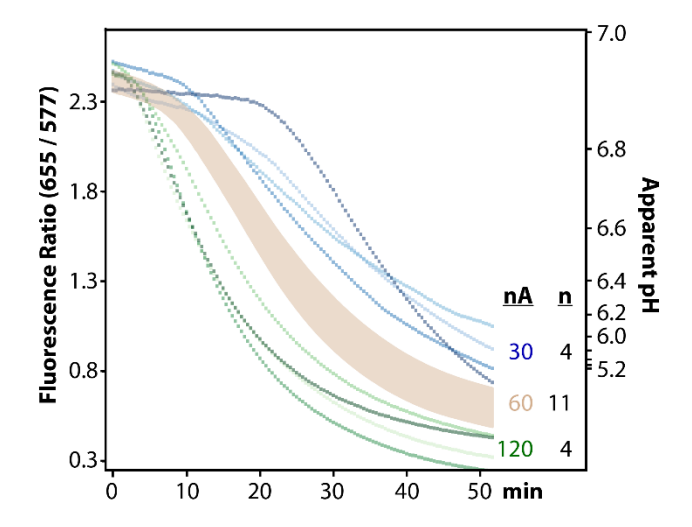


Figure 6. Increasingly large magnitudes of electrospray current (*i.e.*, larger applied potentials) induce increasingly rapid changes in solution pH. A current of 120 nA (green traces) results in decreased solution pH almost immediately, whereas 30 nA (blue traces) results in a period of stability prior to the onset of acidification. Each dotted trace represents a technical replicate (n = 4 for each). The results using 60 nA (transparent beige interval that spans the 95% confidence interval based on 11 technical replicates and is also reported in Figure 5B) are bracketed by the results using lower and higher currents.

Effect of Electrolyte Concentration. Although ammonium acetate has little buffering capacity at neutral pH, it has been suggested that higher concentrations of ammonium acetate will improve its ability to resist changes in pH, but will also increase the formation rate of redox products. ¹⁶ To explore which of these factors are predominant, SNARF-4F was electrosprayed from aqueous ammonium acetate at 10 mM, 200 mM, and 1 M that was adjusted to pH 7.0; this range of concentrations spans that used in most native MS experiments. ^{48,64,65} The results from applying 60 nA of current to SNARF-4F prepared in each of these solutions are shown in Figure 7. The observed trends demonstrate that increasing electrolyte concentration increases the initial

resistance to ESI-induced changes in pH. During region I, the fluorescence ratio decreases >17 times faster in the 10 mM solution than in the 1 M solution. The steep drop in the fluorescence ratio indicates rapid acidification of the 10 mM solution. The 1 M solution exhibits a slope close to zero (-0.008 min⁻¹) during the same period. However, this trend reverses over the course of the experiment. In region II for the 10 mM solution, the change in ratio slows by 70% to -0.04 min⁻¹ relative to region I. The change in ratio slows to -0.01 min⁻¹ and -0.003 min⁻¹ in regions III to IV, respectively. Conversely, the ratios for the 1 M solution are relatively stable through regions I to III. Beyond region III, the fluorescence ratio abruptly drops at a rate >10x faster than the preceding regions, although this is still less than half of the rate observed for 10 mM solutions.

These results indicate that higher electrolyte concentrations in nanoESI applications are more effective at resisting pH changes from electrospray relative to lower electrolyte concentrations. High concentrations of ammonium acetate can also improve the quality of protein mass spectra by reducing the relative abundance of metal ion adducts. However, the concentration of electrolyte can also affect electrostatic interactions in proteins, which in turn can affect the strengths of protein-ligand and protein-protein interactions in solution. Therefore, care should be taken when selecting the electrolyte concentration with respect to the analyte and the relevant biological environment.

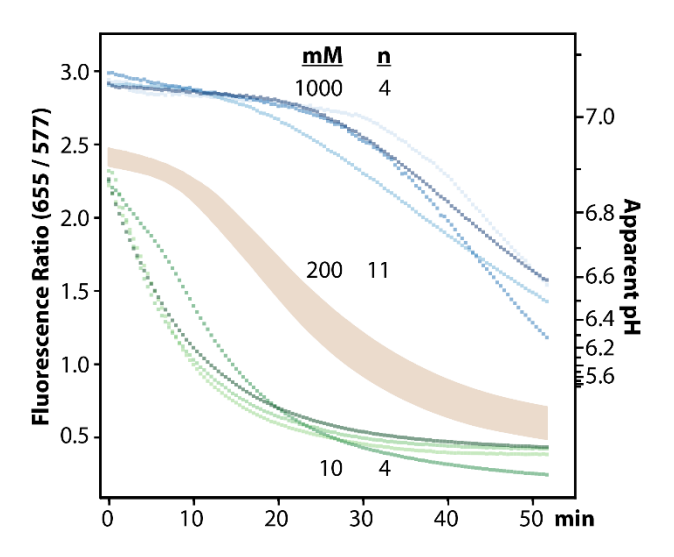


Figure 7. The effect of ammonium acetate concentration on the sample pH as a function of time, based on experiments using a current of 60 nA in positive-ion mode. Aqueous 1 M ammonium acetate solutions (blue traces) exhibit the greatest resistance to changes in pH. Aqueous 10 mM ammonium acetate solutions (green traces) exhibit rapid acidification beginning shortly following the application of a potential. Each dotted trace represents a technical replicate (n = 4 for each). The results using aqueous 200 mM ammonium acetate (transparent beige interval that spans the 95% confidence interval and is also reported in Figure 5B) are bracketed by the results using lower and higher electrolyte concentration.

Effect of Electrospray Polarity. Although most native MS experiments probe native-like cations, experiments probing native-like anions can provide similar⁶⁹ and complementary data.⁵⁶ Therefore, it is useful to understand how the application of positive versus negative potential during electrospray affects the characteristics of the electrospray solution. To do so, we considered the "status quo" conditions described above (Table 1), but under negative polarity. As shown by the black trace in Figure 8, using a negative potential has a far smaller effect on the electrospray solution compared to a positive potential under the same conditions (Figure 5). The

apparent pH of the electrospray solution increases less than 0.1 pH unit under negative polarity, which corresponds to a 25% increase in hydroxide concentration. This is in stark contrast to the more than order of magnitude increase in proton concentration during the corresponding experiments using positive electrospray ionization. For 10 mM electrolyte, using an electrospray current of -60 nA resulted in the fluorescence ratio more than doubling over the course of the experiment, which corresponds to an increase of 0.65 in apparent pH. The fluorescence ratio increases at a rate of +0.087 min⁻¹ through region III and then decreases slightly to +0.055 min⁻¹ for the final 20 minutes. The monotonic increase in fluorescence ratio and apparent pH with negative ionization and 10 mM ammonium acetate is consistent with the solution not reaching the buffering regime of ammonium (p K_a 9.25).

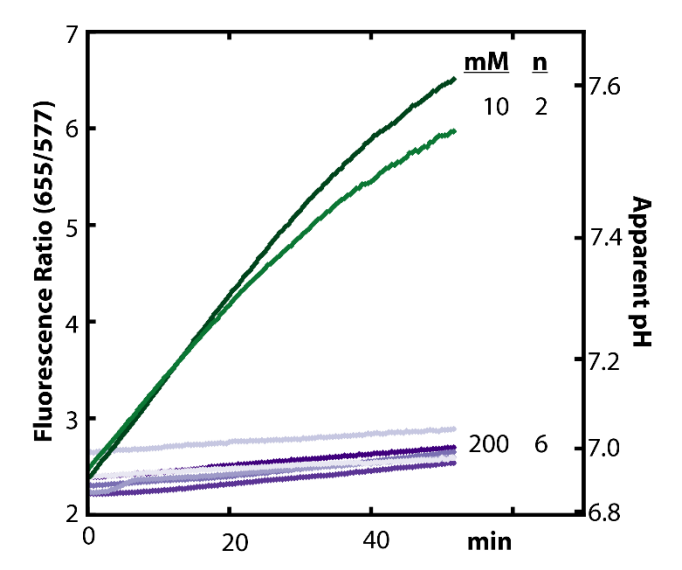


Figure 8. The effect of applying a negative potential on the sample pH as a function of time. Solutions of aqueous 200 mM ammonium acetate and 60 nA under negative polarity (purple traces, n = 6 technical replicates) exhibit a small increase in fluorescence ratio throughout the

experiment. Solutions of aqueous 10 mM ammonium acetate and 60 nA under negative polarity (green traces, n = 2 technical replicates) display modest alkalization.

The minimal alkalization of the 200 mM ammonium acetate solution is less straightforward to explain. With a platinum electrode, water oxidation and reduction should be the primary source of charge balance and redox-induced changes in pH under positive and negative polarity, respectively.³¹ Because water can undergo many possible redox reactions that vary in reduction potential (and therefore probability of occurrence),³¹ it is plausible that the reduction reactions occurring under negative-mode ionization produce fewer pH-altering species,³¹ which would account for smaller overall change in solution composition over the timeframe of the experiment. It is likely that many reactions take place during these experiments²⁷ and a thorough understanding of this phenomenon will require further investigation.

Conclusions

Figure 4 shows an example of how the features in native mass spectra can evolve during individual experiments, which we hypothesized was caused by electrochemically induced acidification of samples concomitant with positive-polarity ESI. Ratiometric fluorescence imaging experiments (Figures 2 and 3) provide compelling evidence that sample pH can drift (Figure 5) during native MS experiments, which typically use even smaller sample volumes than used here (10 μL). For positive-polarity nanoESI of samples of a given electrolyte concentration, increasing the ionization current increased the rate of sample acidification (Figure 6). Samples with higher electrolyte concentrations are more resistant to changes in pH during nanoESI (Figure 7), but electrolyte concentration also affects electrostatic interactions in solution.

Negative-polarity nanoESI results in slower changes in solution pH than analogous experiments performed using positive polarity (Figure 8).

Based on these results and observations, we suspect that sample pH can drift during many native MS experiments. Because the properties of many proteins depend strongly on pH, it is likely that results of many native MS experiments have been affected by this phenomenon. We recommend that researchers consider the following during the design and analysis of native MS experiments: (1) Favor parameters (*e.g.*, high electrolyte concentrations, negative polarity ionization, and low ionization currents that mitigate changes in pH during experiments. (2) Acquire data using positive and negative polarity. Because the pH of the samples in those experiments would change in opposite directions, similar results (*e.g.*, stoichiometry, equilibria constants, collision cross sections, etc.) for the two polarities would be consistent with the results being independent of any changes in pH that may have occurred. (3) Compare data acquired at different intervals (*e.g.*, near the beginning and near the end) during the same nanoESI experiment. Because the pH of the samples depends on time, similar results for different time intervals would be consistent with the results being independent of any changes in pH that occurred.

Supporting Information. Additional Description of Apparatus, Assessment of Measurement Variability, and Figure S1.

Acknowledgments. This work was supported by the National Science Foundation through awards 1807382 and 2203513 from the Division of Chemistry, with partial co-funding from the Division of Molecular and Cellular Biosciences.

509 References

- 510 (1) Fenn, J. B.; Mann, M.; Meng, C. K.; Wong, S. F.; Whitehouse, C. M. Electrospray
- Ionization for Mass Spectrometry of Large Biomolecules. Science 1989, 246 (4926), 64–
- 512 71. https://doi.org/10.1126/science.2675315.
- 513 (2) Davidson, K. L.; Oberreit, D. R.; Hogan, C. J.; Bush, M. F. Nonspecific Aggregation in
- Native Electrokinetic Nanoelectrospray Ionization. *Int. J. Mass Spectrom.* **2017**, *420*
- 515 (Supplement C), 35–42. https://doi.org/10.1016/j.ijms.2016.09.013.
- 516 (3) Wilm, M. S.; Mann, M. Electrospray and Taylor-Cone Theory, Dole's Beam of
- Macromolecules at Last? Int. J. Mass Spectrom. Ion Process. 1994, 136 (2), 167–180.
- 518 https://doi.org/10.1016/0168-1176(94)04024-9.
- 519 (4) Wilm, M.; Mann, M. Analytical Properties of the Nanoelectrospray Ion Source. Anal.
- 520 Chem. **1996**, 68 (1), 1–8. https://doi.org/10.1021/ac9509519.
- 521 (5) Karas, M.; Bahr, U.; Dülcks, T. Nano-Electrospray Ionization Mass Spectrometry:
- Addressing Analytical Problems beyond Routine. Fresenius J. Anal. Chem. 2000, 366 (6),
- 523 669–676. https://doi.org/10.1007/s002160051561.
- 524 (6) Juraschek, R.; Dülcks, T.; Karas, M. Nanoelectrospray—More than Just a Minimized-
- Flow Electrospray Ionization Source. J. Am. Soc. Mass Spectrom. 1999, 10 (4), 300–308.
- 526 https://doi.org/10.1021/jasms.8b01315.
- 527 (7) El-Faramawy, A.; Siu, K. W. M.; Thomson, B. A. Efficiency of Nano-Electrospray
- 528 Ionization. J. Am. Soc. Mass Spectrom. **2005**, 16 (10), 1702–1707.
- 529 https://doi.org/10.1016/j.jasms.2005.06.011.

- 530 (8) Tang, X.; Bruce, J. E.; Hill, H. H. Characterizing Electrospray Ionization Using
- Atmospheric Pressure Ion Mobility Spectrometry. *Anal. Chem.* **2006**, *78* (22), *7751–7760*.
- 532 https://doi.org/10.1021/ac0613380.
- 533 (9) Leney, A. C.; Heck, A. J. R. Native Mass Spectrometry: What Is in the Name? J. Am. Soc.
- 534 *Mass Spectrom.* **2017**, 28 (1), 5–13. https://doi.org/10.1007/s13361-016-1545-3.
- 535 (10) Gault, J.; Liko, I.; Landreh, M.; Shutin, D.; Bolla, J. R.; Jefferies, D.; Agasid, M.; Yen, H.-
- Y.; Ladds, M. J. G. W.; Lane, D. P.; Khalid, S.; Mullen, C.; Remes, P. M.; Huguet, R.;
- McAlister, G.; Goodwin, M.; Viner, R.; Syka, J. E. P.; Robinson, C. V. Combining Native
- and "omics" Mass Spectrometry to Identify Endogenous Ligands Bound to Membrane
- Proteins. Nat. Methods **2020**, 17 (5), 505–508. https://doi.org/10.1038/s41592-020-0821-
- 540 0.
- 541 (11) Benesch, J. L. P.; Ruotolo, B. T.; Simmons, D. A.; Robinson, C. V. Protein Complexes in
- the Gas Phase: Technology for Structural Genomics and Proteomics. *Chem. Rev.* **2007**,
- 543 107 (8), 3544–3567. https://doi.org/10.1021/cr068289b.
- 544 (12) Reijenga, J.; van Hoof, A.; van Loon, A.; Teunissen, B. Development of Methods for the
- Determination of PK a Values. Anal. Chem. Insights 2013, 8, ACI.S12304.
- 546 https://doi.org/10.4137/ACI.S12304.
- 547 (13) Marek, P. J.; Patsalo, V.; Green, D. F.; Raleigh, D. P. Ionic Strength Effects on Amyloid
- Formation by Amylin Are a Complicated Interplay among Debye Screening, Ion
- Selectivity, and Hofmeister Effects. *Biochemistry* **2012**, *51* (43), 8478–8490.
- 550 https://doi.org/10.1021/bi300574r.

- 551 (14) Nørby, J. G.; Esmann, M. The Effect of Ionic Strength and Specific Anions on Substrate
- Binding and Hydrolytic Activities of Na,K-ATPase. J. Gen. Physiol. 1997, 109 (5), 555–
- 553 570. https://doi.org/10.1085/jgp.109.5.555.
- 554 (15) Stoll, V. S.; Blanchard, J. S. Chapter 6 Buffers: Principles and Practice 1. In Methods in
- Enzymology; Burgess, R. R., Deutscher, M. P., Eds.; Guide to Protein Purification, 2nd
- 556 Edition; Academic Press, 2009; Vol. 463, pp 43–56. https://doi.org/10.1016/S0076-
- 557 6879(09)63006-8.
- 558 (16) Konermann, L. Addressing a Common Misconception: Ammonium Acetate as Neutral PH
- "Buffer" for Native Electrospray Mass Spectrometry. J. Am. Soc. Mass Spectrom. 2017,
- 560 28 (9), 1827–1835. https://doi.org/10.1007/s13361-017-1739-3.
- 561 (17) Susa, A. C.; Xia, Z.; Williams, E. R. Small Emitter Tips for Native Mass Spectrometry of
- Proteins and Protein Complexes from Nonvolatile Buffers That Mimic the Intracellular
- 563 Environment. Anal. Chem. **2017**, 89 (5), 3116–3122.
- 564 https://doi.org/10.1021/acs.analchem.6b04897.
- 565 (18) Nguyen, G. T. H.; Tran, T. N.; Podgorski, M. N.; Bell, S. G.; Supuran, C. T.; Donald, W.
- A. Nanoscale Ion Emitters in Native Mass Spectrometry for Measuring Ligand–Protein
- 567 Binding Affinities. ACS Cent. Sci. **2019**, 5 (2), 308–318.
- 568 https://doi.org/10.1021/acscentsci.8b00787.
- 569 (19) Jordan, J. S.; Williams, E. R. Effects of Electrospray Droplet Size on Analyte
- Aggregation: Evidence for Serine Octamer in Solution. *Anal. Chem.* **2021**, *93* (3), 1725–
- 571 1731. https://doi.org/10.1021/acs.analchem.0c04343.

- 572 (20) Mortensen, D. N.; Williams, E. R. Surface-Induced Protein Unfolding in Submicron
- 573 Electrospray Emitters. *Anal. Chem.* **2016**, *88* (19), 9662–9668.
- 574 https://doi.org/10.1021/acs.analchem.6b02499.
- 575 (21) Hedges, J. B.; Vahidi, S.; Yue, X.; Konermann, L. Effects of Ammonium Bicarbonate on
- 576 the Electrospray Mass Spectra of Proteins: Evidence for Bubble-Induced Unfolding. *Anal.*
- 577 Chem. **2013**, 85 (13), 6469–6476. https://doi.org/10.1021/ac401020s.
- 578 (22) Cassou, C. A.; Williams, E. R. Anions in Electrothermal Supercharging of Proteins with
- 579 Electrospray Ionization Follow a Reverse Hofmeister Series. *Anal. Chem.* **2014**, *86* (3),
- 580 1640–1647. https://doi.org/10.1021/ac403398j.
- 581 (23) Konermann, L.; Ahadi, E.; Rodriguez, A. D.; Vahidi, S. Unraveling the Mechanism of
- 582 Electrospray Ionization. *Anal. Chem.* **2013**, *85* (1), 2–9.
- 583 https://doi.org/10.1021/ac302789c.
- 584 (24) Zhou, S.; Edwards, A. G.; Cook, K. D.; Van Berkel, G. J. Investigation of the Electrospray
- Plume by Laser-Induced Fluorescence Spectroscopy. *Anal. Chem.* **1999**, *71* (4), 769–776.
- 586 https://doi.org/10.1021/ac981259r.
- 587 (25) Jackson, G. S.; Enke, C. G. Electrical Equivalence of Electrospray Ionization with
- 588 Conducting and Nonconducting Needles. *Anal. Chem.* **1999**, *71* (17), 3777–3784.
- 589 https://doi.org/10.1021/ac9902244.
- 590 (26) Kebarle, P.; Verkerk, U. H. Electrospray: From Ions in Solution to Ions in the Gas Phase,
- What We Know Now. *Mass Spectrom. Rev.* **2009**, *28* (6), 898–917.
- 592 https://doi.org/10.1002/mas.20247.
- 593 (27) Van Berkel, G. J.; Zhou, F.; Aronson, J. T. Changes in Bulk Solution PH Caused by the
- Inherent Controlled-Current Electrolytic Process of an Electrospray Ion Source. *Int. J.*

- 595 *Mass Spectrom. Ion Process.* **1997**, *162* (1–3), 55–67. https://doi.org/10.1016/S0168-
- 596 1176(96)04476-X.
- 597 (28) Berkel, G. J. V. Electrolytic Corrosion of a Stainless-Steel Electrospray Emitter Monitored
- Using an Electrospray–Photodiode Array System. J. Anal. At. Spectrom. 1998, 13 (7),
- 599 603–607. https://doi.org/10.1039/A800373D.
- 600 (29) Fernandez de la Mora, J.; Van Berkel, G. J.; Enke, C. G.; Cole, R. B.; Martinez-Sanchez,
- M.; Fenn, J. B. Electrochemical Processes in Electrospray Ionization Mass Spectrometry.
- 602 J. Mass Spectrom. 2000, 35 (8), 939–952. https://doi.org/10.1002/1096-
- 603 9888(200008)35:8<939::AID-JMS36>3.0.CO;2-V.
- 604 (30) Van Berkel, G. J.; Asano, K. G.; Schnier, P. D. Electrochemical Processes in a Wire-in-a-
- 605 Capillary Bulk-Loaded, Nano-Electrospray Emitter. J. Am. Soc. Mass Spectrom. 2001, 12
- 606 (7), 853–862. https://doi.org/10.1016/S1044-0305(01)00264-1.
- 607 (31) Van Berkel, G. J.; Kertesz, V. Using the Electrochemistry of the Electrospray Ion Source.
- 608 Anal. Chem. **2007**, 79 (15), 5510–5520. https://doi.org/10.1021/ac071944a.
- 609 (32) Pozniak, B. P.; Cole, R. B. Perspective on Electrospray Ionization and Its Relation to
- 610 Electrochemistry. J. Am. Soc. Mass Spectrom. **2015**, 26 (3), 369–385.
- 611 https://doi.org/10.1007/s13361-014-1066-x.
- 612 (33) Blades, A. T.; Ikonomou, M. G.; Kebarle, Paul. Mechanism of Electrospray Mass
- Spectrometry. Electrospray as an Electrolysis Cell. Anal. Chem. 1991, 63 (19), 2109–
- 614 2114. https://doi.org/10.1021/ac00019a009.
- 615 (34) Van Berkel, G. J.; Zhou, F. Characterization of an Electrospray Ion Source as a
- 616 Controlled-Current Electrolytic Cell. *Anal. Chem.* **1995**, *67* (17), 2916–2923.
- 617 https://doi.org/10.1021/ac00113a028.

- 618 (35) Pei, J.; Zhou, X.; Wang, X.; Huang, G. Alleviation of Electrochemical Oxidation for
- Peptides and Proteins in Electrospray Ionization: Obtaining More Accurate Mass Spectra
- 620 with Induced High Voltage. *Anal. Chem.* **2015**, 87 (5), 2727–2733.
- 621 https://doi.org/10.1021/ac503990a.
- 622 (36) Dupont, A.; Gisselbrecht, J.-P.; Leize, E.; Wagner, L.; Van Dorsselaer, A. Electrospray
- Mass Spectrometry of Electrochemically Ionized Molecules: Application to the Study of
- Fullerenes. Tetrahedron Lett. **1994**, 35 (33), 6083–6086. https://doi.org/10.1016/0040-
- 625 4039(94)88081-6.
- 626 (37) Hop, C. E.; Saulys, D. A.; Gaines, D. F. Electrospray Mass Spectrometry of Borane Salts:
- The Electrospray Needle as an Electrochemical Cell. J. Am. Soc. Mass Spectrom. 1995, 6
- 628 (9), 860–865. https://doi.org/10.1016/1044-0305(95)00478-V.
- 629 (38) Guaratini, T.; Vessecchi, R.; Pinto, E.; Colepicolo, P.; Lopes, N. P. Balance of
- Xanthophylls Molecular and Protonated Molecular Ions in Electrospray Ionization. *J.*
- 631 *Mass Spectrom.* **2005**, 40 (7), 963–968. https://doi.org/10.1002/jms.874.
- 632 (39) Xu, Xiaoming.; Nolan, S. P.; Cole, R. B. Electrochemical Oxidation and Nucleophilic
- Addition Reactions of Metallocenes in Electrospray Mass Spectrometry. *Anal. Chem.*
- 634 **1994**, 66 (1), 119–125. https://doi.org/10.1021/ac00073a021.
- 635 (40) Rondeau, D.; Kreher, D.; Cariou, M.; Hudhomme, P.; Gorgues, A.; Richomme, P.
- Electrolytic Electrospray Ionization Mass Spectrometry of C60-TTF-C60 Derivatives:
- High-Resolution Mass Measurement and Molecular Ion Gas-Phase Reactivity. *Rapid*
- 638 Commun. Mass Spectrom. **2001**, 15 (18), 1708–1712. https://doi.org/10.1002/rcm.423.
- 639 (41) Zhou, S.; Prebyl, B. S.; Cook, K. D. Profiling PH Changes in the Electrospray Plume.
- 640 Anal. Chem. 2002, 74 (19), 4885–4888. https://doi.org/10.1021/ac025960d.

- 641 (42) Gatlin, C. L.; Turecek, Frantisek. Acidity Determination in Droplets Formed by
- Electrospraying Methanol-Water Solutions. *Anal. Chem.* **1994**, *66* (5), 712–718.
- 643 https://doi.org/10.1021/ac00077a021.
- 644 (43) Rajagopal, P.; Tse, E.; Borst, A. J.; Delbecq, S. P.; Shi, L.; Southworth, D. R.; Klevit, R.
- E. A Conserved Histidine Modulates HSPB5 Structure to Trigger Chaperone Activity in
- Response to Stress-Related Acidosis. *eLife* **2015**, *4*, e07304.
- 647 https://doi.org/10.7554/eLife.07304.
- 648 (44) Santambrogio, C.; Natalello, A.; Brocca, S.; Ponzini, E.; Grandori, R. Conformational
- 649 Characterization and Classification of Intrinsically Disordered Proteins by Native Mass
- Spectrometry and Charge-State Distribution Analysis. *Proteomics* **2019**, *19* (6), e1800060.
- https://doi.org/10.1002/pmic.201800060.
- 652 (45) Santos, J.; Iglesias, V.; Santos-Suárez, J.; Mangiagalli, M.; Brocca, S.; Pallarès, I.;
- Ventura, S. PH-Dependent Aggregation in Intrinsically Disordered Proteins Is Determined
- by Charge and Lipophilicity. *Cells* **2020**, *9* (1). https://doi.org/10.3390/cells9010145.
- 655 (46) Meyer, T.; Gabelica, V.; Grubmüller, H.; Orozco, M. Proteins in the Gas Phase. WIREs
- 656 *Comput. Mol. Sci.* **2013**, *3* (4), 408–425. https://doi.org/10.1002/wcms.1130.
- 657 (47) Chingin, K.; Barylyuk, K.; Chen, H. On the Preservation of Non-Covalent Protein
- 658 Complexes during Electrospray Ionization. *Philos. Transact. A Math. Phys. Eng. Sci.*
- 659 **2016**, 374 (2079). https://doi.org/10.1098/rsta.2015.0377.
- 660 (48) Gadzuk-Shea, M. M.; Bush, M. F. Effects of Charge State on the Structures of Serum
- Albumin Ions in the Gas Phase: Insights from Cation-to-Anion Proton-Transfer Reactions,
- 662 Ion Mobility, and Mass Spectrometry. J. Phys. Chem. B **2018**, 122 (43), 9947–9955.
- https://doi.org/10.1021/acs.jpcb.8b08427.

- 664 (49) Giles, K.; Ujma, J.; Wildgoose, J.; Pringle, S.; Richardson, K.; Langridge, D.; Green, M.
- A Cyclic Ion Mobility-Mass Spectrometry System. Anal. Chem. 2019, 91 (13), 8564
- 8573. https://doi.org/10.1021/acs.analchem.9b01838.
- 667 (50) Liu, J.; Diwu, Z.; Leung, W.-Y. Synthesis and Photophysical Properties of New
- Fluorinated Benzo[c]Xanthene Dyes as Intracellular PH Indicators. *Bioorg. Med. Chem.*
- 669 Lett. **2001**, 11 (22), 2903–2905. https://doi.org/10.1016/S0960-894X(01)00595-9.
- 670 (51) Marcotte, N.; Brouwer, A. M. Carboxy SNARF-4F as a Fluorescent PH Probe for
- Ensemble and Fluorescence Correlation Spectroscopies. J. Phys. Chem. B 2005, 109 (23),
- 672 11819–11828. https://doi.org/10.1021/jp0510138.
- 673 (52) Raimondo, J. V.; Irkle, A.; Wefelmeyer, W.; Newey, S. E.; Akerman, C. J. Genetically
- Encoded Proton Sensors Reveal Activity-Dependent PH Changes in Neurons. Front. Mol.
- 675 *Neurosci.* **2012**, *5*. https://doi.org/10.3389/fnmol.2012.00068.
- 676 (53) Senear, D. F.; Teller, D. C. Thermodynamics of Concanavalin A Dimer-Tetramer Self-
- Association: Sedimentation Equilibrium Studies. *Biochemistry* **1981**, *20* (11), 3076–3083.
- 678 https://doi.org/10.1021/bi00514a014.
- 679 (54) Boeri Erba, E.; Barylyuk, K.; Yang, Y.; Zenobi, R. Quantifying Protein-Protein
- Interactions Within Noncovalent Complexes Using Electrospray Ionization Mass
- Spectrometry. Anal. Chem. **2011**, 83 (24), 9251–9259. https://doi.org/10.1021/ac201576e.
- 682 (55) Tian, Y.; Han, L.; Buckner, A. C.; Ruotolo, B. T. Collision Induced Unfolding of Intact
- Antibodies: Rapid Characterization of Disulfide Bonding Patterns, Glycosylation, and
- 684 Structures. Anal. Chem. 2015, 87 (22), 11509–11515.
- https://doi.org/10.1021/acs.analchem.5b03291.

- 686 (56) Hong, S.; Bush, M. F. Collision-Induced Unfolding Is Sensitive to the Polarity of Proteins
- and Protein Complexes. J. Am. Soc. Mass Spectrom. **2019**, 30 (11), 2430–2437.
- 688 https://doi.org/10.1021/jasms.8b06263.
- 689 (57) Benesch, J. L. P.; Sobott, F.; Robinson, C. V. Thermal Dissociation of Multimeric Protein
- 690 Complexes by Using Nanoelectrospray Mass Spectrometry. *Anal. Chem.* **2003**, 75 (10),
- 691 2208–2214. https://doi.org/10.1021/ac034132x.
- 692 (58) Zhang, J.; Malmirchegini, G. R.; Clubb, R. T.; Loo, J. A. Native Top-down Mass
- Spectrometry for the Structural Characterization of Human Hemoglobin. Eur. J. Mass
- 694 Spectrom. **2015**, 21 (3), 221–231. https://doi.org/10.1255/ejms.1340.
- 695 (59) Kulkarni, R. P.; Mishra, S.; Fraser, S. E.; Davis, M. E. Single Cell Kinetics of
- Intracellular, Nonviral, Nucleic Acid Delivery Vehicle Acidification and Trafficking.
- 697 Bioconjug. Chem. **2005**, 16 (4), 986–994. https://doi.org/10.1021/bc050081u.
- 698 (60) Waser, J. Acid-Base Titration and Distribution Curves. J. Chem. Educ. 1967, 44 (5), 274.
- 699 https://doi.org/10.1021/ed044p274.
- 700 (61) Hernández, H.; Robinson, C. V. Determining the Stoichiometry and Interactions of
- Macromolecular Assemblies from Mass Spectrometry. *Nat. Protoc.* **2007**, *2* (3), 715–726.
- 702 https://doi.org/10.1038/nprot.2007.73.
- 703 (62) Thompson, N. J.; Rosati, S.; Heck, A. J. R. Performing Native Mass Spectrometry
- Analysis on Therapeutic Antibodies. *Methods* **2014**, *65* (1), 11–17.
- 705 https://doi.org/10.1016/j.ymeth.2013.05.003.
- 706 (63) Schmidt, A.; Karas, M.; Dülcks, T. Effect of Different Solution Flow Rates on Analyte Ion
- Signals in Nano-ESI MS, or: When Does ESI Turn into Nano-ESI? J. Am. Soc. Mass
- 708 Spectrom. **2003**, 14 (5), 492–500. https://doi.org/10.1016/S1044-0305(03)00128-4.

- 709 (64) Chen, S.-H.; Russell, D. H. How Closely Related Are Conformations of Protein Ions
- Sampled by IM-MS to Native Solution Structures? J. Am. Soc. Mass Spectrom. 2015, 26
- 711 (9), 1433–1443. https://doi.org/10.1007/s13361-015-1191-1.
- 712 (65) Sterling, H. J.; Batchelor, J. D.; Wemmer, D. E.; Williams, E. R. Effects of Buffer
- Loading for Electrospray Ionization Mass Spectrometry of a Noncovalent Protein
- 714 Complex That Requires High Concentrations of Essential Salts. J. Am. Soc. Mass
- 715 Spectrom. **2010**, 21 (6), 1045–1049. https://doi.org/10.1016/j.jasms.2010.02.003.
- 716 (66) Iavarone, A. T.; Udekwu, O. A.; Williams, E. R. Buffer Loading for Counteracting Metal
- 717 Salt-Induced Signal Suppression in Electrospray Ionization. *Anal. Chem.* **2004**, *76* (14),
- 718 3944–3950. https://doi.org/10.1021/ac049724+.
- 719 (67) Gavriilidou, A. F. M.; Gülbakan, B.; Zenobi, R. Influence of Ammonium Acetate
- Concentration on Receptor–Ligand Binding Affinities Measured by Native Nano ESI-MS:
- 721 A Systematic Study. *Anal. Chem.* **2015**, 87 (20), 10378–10384.
- 722 https://doi.org/10.1021/acs.analchem.5b02478.
- 723 (68) Zhou, M.; Sandercock, A. M.; Fraser, C. S.; Ridlova, G.; Stephens, E.; Schenauer, M. R.;
- Yokoi-Fong, T.; Barsky, D.; Leary, J. A.; Hershey, J. W.; Doudna, J. A.; Robinson, C. V.
- Mass Spectrometry Reveals Modularity and a Complete Subunit Interaction Map of the
- 726 Eukaryotic Translation Factor EIF3. *Proc. Natl. Acad. Sci.* **2008**, *105* (47), 18139–18144.
- 727 https://doi.org/10.1073/pnas.0801313105.
- 728 (69) Allen, S. J.; Schwartz, A. M.; Bush, M. F. Effects of Polarity on the Structures and Charge
- 729 States of Native-Like Proteins and Protein Complexes in the Gas Phase. *Anal. Chem.*
- 730 **2013**, *85*, 12055–12061. https://doi.org/10.1021/ac403139d.

732 For TOC Only

